Green Chemistry

Aqueous phase synthesis of benzyl ester over partially thiolated Au_{25} nanocluster catalysts: improving selectivity with hydrophobic carbon support

Journal:	*Green Chemistry*
Manuscript ID	GC-ART-03-2025-001292.R1
Article Type:	Paper
Date Submitted by the Author:	30-Apr-2025
Complete List of Authors:	Sakamoto, Kosuke ; The University of Tokyo, Department of Chemistry, Graduate School of Science Chida, Koki; Tohoku University, Masuda, Shinya; The University of Tokyo, Department of Chemistry, School of Science Yoshii, Takeharu; Tohoku University, Institute of Multidisciplinary Research for Advanced Materials Nishihara, Hirotomo; Tohoku University, Institute of Multidisciplinary Research for Advanced Materials Tsukuda, Tatsuya; The University of Tokyo, Department of Chemistry, School of Science

Green foundation box

1. Esters are important intermediates in pharmaceutical chemistry, but their synthetic method requires excess nucleophilic alcohols and complete removal of water to prevent hydrolysis of esters. This work proposes an alternative catalytic route that can synthesize esters in water without the addition of excess alcohols.
2. We demonstrated that the benzyl benzoate ester can be formed as the main product in aqueous phase when using Au nanocluster catalyst supported on hydrophobic carbon. By constructing similar active Au sites on each carbon support, which is challenging in the conventional synthesis method, we clarified that the carbon without the functional groups can enhance the ester selectivity and proposed a design principle for synthesizing further effective catalysts.
3. Further improvement in the ester yield and expansion of the substrate scope in the aqueous conditions is desired.

ARTICLE

Aqueous phase synthesis of benzyl ester over partially thiolated Au_{25} nanocluster catalysts: improving selectivity with hydrophobic carbon support

Received 00th January 20xx,
Accepted 00th January 20xx

DOI: 10.1039/x0xx00000x

Kosuke Sakamoto,[a] Koki Chida,[b] Shinya Masuda,*[a] Takeharu Yoshii,*[b] Hirotomo Nishihara[b,c] and Tatsuya Tsukuda*[a]

The aqueous phase synthesis of esters via oxidative coupling of the alcohols catalyzed by carbon-supported gold catalysts is one of the environmentally benign approaches, but remains challenging. To understand the role of the carbon support in maximizing the selectivity to esters, we have here deposited partially thiolated Au_{25} nanoclusters as common reactive centers on three types of carbon supports: commercially available porous carbon (CNovel), carbon mesosponge (CMS), and graphene mesosponge (GMS). These carbons have similar porous structures but significantly different amounts of functional groups. When GMS with the fewest functional groups was used as support, the Au_{25} nanocluster catalysts exhibited the highest selectivity towards benzyl benzoate in the oxidation of benzyl alcohol in aqueous conditions, with a maximum yield of 67% under the optimized conditions. Mechanistic studies revealed that the carbon supports, due to their hydrophobic nature, played two crucial roles in the unique selectivity: (i) protection of the intermediate benzaldehyde from nucleophilic attack by hydroxy ions while facilitating the attack by alkoxide, and (ii) adsorption of benzyl benzoates on the support to prevent hydrolysis.

Introduction

Esters are important chemicals in the field of synthetic and pharmaceutical chemistry.[1–6] The conventional synthesis of esters involves the dehydrative coupling of a carboxylic acid and an alcohol under acidic conditions (Scheme 1a).[7] However, this route requires excess acids, which is unfavorable from a green chemistry perspective. Therefore, there is a need to develop catalysts that are not only selective but also environmentally benign. Gold nanoparticles (AuNPs) are known to serve as catalysts for ester synthesis from alcohols in the presence of a base (Scheme 1b):[8,9] an alcohol is first oxidized to the aldehyde,[10–17] followed by the nucleophilic attack of the deprotonated alcohol to form the corresponding ester.[18–25] This process is greener than that in Scheme 1a because it uses O_2 as the oxidant and produces water as the only by-product. A disadvantage of this process is the use of a solvent amount of nucleophilic alcohol.

Both of the above processes share the common limitation of requiring anhydrous conditions to prevent hydrolysis of the ester to the corresponding carboxylic acid. Therefore, the catalytic synthesis of esters in water is one of the most challenging processes in green chemistry. Recently, aqueous phase synthesis of esters has been achieved by using biocatalysts or molecular catalysts in the hydrophobic core of the micelles.[26–32] It has also been reported that benzyl benzoate ($PhCOOCH_2Ph$) was obtained from benzyl alcohol ($PhCH_2OH$) in water using gold nanoclusters (AuNCs) supported on carbon[33,34] and AuNPs supported on carbon nanotubes (CNTs) (Scheme 1c).[35] These studies have shown that hydrophobic carbon supports play a key role in the Au-catalyzed ester synthesis in water. However, the factors that maximize ester yield have not been elucidated because the size of AuNCs and AuNPs varied significantly depending on the carbon support used.

This study aims to answer the question of how the structures of the carbon supports affect the catalytic performance of Au catalysts for ester synthesis in the aqueous phase. For this purpose, it is necessary to prepare robust AuNCs of the common size on different carbon supports. Such heterogeneous AuNC catalysts can be synthesized by partial or complete removal of the protecting ligands from atomically-precise, ligand-protected AuNCs adsorbed on solid supports.[36–53] The resulting AuNC catalysts with partial ligand removal showed higher durability than ligand-free AuNCs due to multiple non-covalent interactions between the remaining ligands and the support.[34,54,55] Here, we synthesized the partially thiolated Au_{25} NCs on three types of mesoporous carbon supports: commercially available porous carbon (CNovel), carbon mesosponge (CMS), and graphene mesosponge (GMS), which have similar porous structures but significantly different amounts of functional groups, such as phenol, ether, carbonyl, carboxylic acid and carboxylic anhydride.[56–59] We hypothesized that the reducing the amount of hydrophilic surface functional groups would alter the hydrophobicity of the carbon surface, resulting in better ester selectivity in the aqueous phase. The catalytic properties of these catalysts were

[a] Department of Chemistry, Graduate School of Science, The University of Tokyo, 7-3-1 Hongo, Bunkyo-ku, Tokyo 113-0033, Japan.
[b] Institute of Multidisciplinary Research for Advanced Materials, Tohoku University, 2-1-1 Katahira, Aoba-ku, Sendai, Miyagi 980-8577, Japan.
[c] Advanced Institute for Materials Research (WPI-AIMR), Tohoku University, 2-1-1 Katahira, Aoba-ku, Sendai, Miyagi 980-8577, Japan.
Electronic supplementary information (ESI) available. See DOI: https://doi.org/10.1039/x0xx00000x

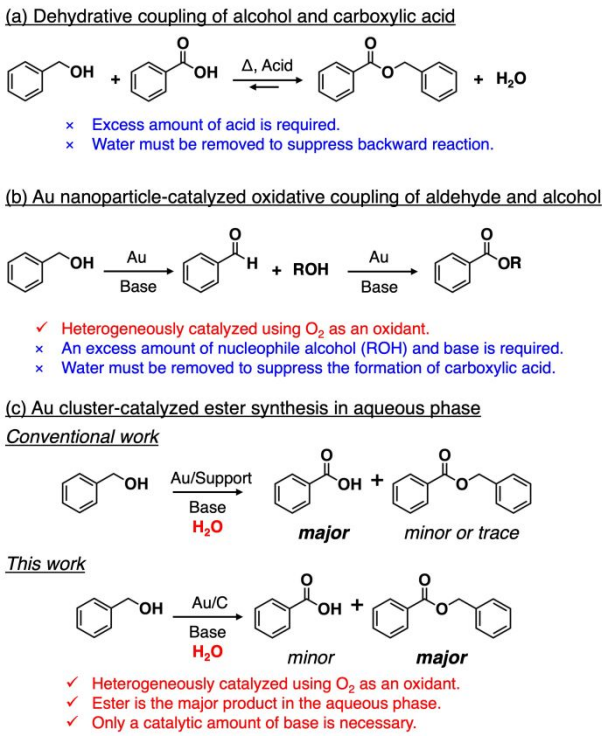

Scheme 1 Comparison of esterification reactions in the previous reports and our work.

compared for the synthesis of $PhCOOCH_2Ph$ from $PhCH_2OH$ in water (Scheme 1c). It was found that the partially thiolated Au_{25} NCs on GMS, the carbon support with almost no functional groups, exhibited the highest selectivity to $PhCOOCH_2Ph$ than those on CMS or CNovel. The maximum $PhCOOCH_2Ph$ yield reached up to ~67% under the optimized conditions. Mechanistic studies suggested that the hydrophobic environment provided by the carbon supports prevents the nucleophilic attack of OH^- to the aldehyde and protects $PhCOOCH_2Ph$ from hydrolysis. This work demonstrates the synergy of active AuNCs and hydrophobic carbon support for an environmentally benign approach to ester synthesis in water.

Results and discussion

Synthesis and characterization of catalysts

$[Au_{25}(PET)_{18}]^0$ (PET = 2-phenylethanethiolate) (Fig. 1A) was synthesized according to the reported procedure.[60] The successful synthesis of $[Au_{25}(PET)_{18}]^0$ was confirmed by negative mode matrix-assisted laser desorption/ionization mass spectrometry (MALDI-MS) (Fig. S1A), ultraviolet-visible (UV-vis) spectroscopy (Fig. S1B), and thermogravimetric (TG) analysis (Fig. S1C).[61] Three types of carbon supports, CNovel, CMS and GMS (Fig. 1B), were used as supports. CNovel is a commercially available porous carbon. CMS was synthesized by a chemical vapor deposition of carbon on an Al_2O_3 template, followed by removal of the Al_2O_3, while GMS was obtained by graphitization of CMS at high temperature.[57–59] These carbon supports were characterized by N_2 adsorption/desorption measurements and temperature-programmed desorption mass spectrometry (TPD-MS).[62–64] The specific surface areas of CNovel, CMS and GMS estimated by N_2 sorption measurement and the Brunauer-Emmett-Teller (BET) method were 2041, 2023 and 1738 $m^2 g^{-1}$, respectively (Fig. 1B and S2A).[65] The total pore volumes of CNovel, CMS and GMS were 3.97, 3.45 and 3.08 $cm^3 g^{-1}$, respectively (Fig. 1B and S2A). The majority of the pores are mesopores (80, 79 and 80% for CNovel, CMS and GMS, respectively) (Fig. 1B and Table S1), and the pore size distributions derived by the Barrett-Joyner-Halenda (BJH) method were comparable (Fig. S2B and Table S1). These results suggest that the three carbons have similar mesoporous structures. In contrast, the total amounts of gas evolved from three carbons during the TPD-MS measurement, which reflect the amount of edge sites on the carbon surface, were significantly different: 3.8, 1.3 and 0.1 mmol g^{-1} for CNovel, CMS, and GMS, respectively (Fig. 1B and S3). Thus, the total amount of functional groups on the carbon surface decreased significantly in the order of CNovel > CMS > GMS.

$[Au_{25}(PET)_{18}]^0$ was adsorbed onto these carbon supports by mixing them in toluene at 0 °C. The loading amount was adjusted to 1 wt% based on the amount of Au. Regardless of the carbon support, the UV-vis spectra of the filtrate after the adsorption showed no peaks of $[Au_{25}(PET)_{18}]^0$ (Fig. S4), indicating that 1 wt% Au of

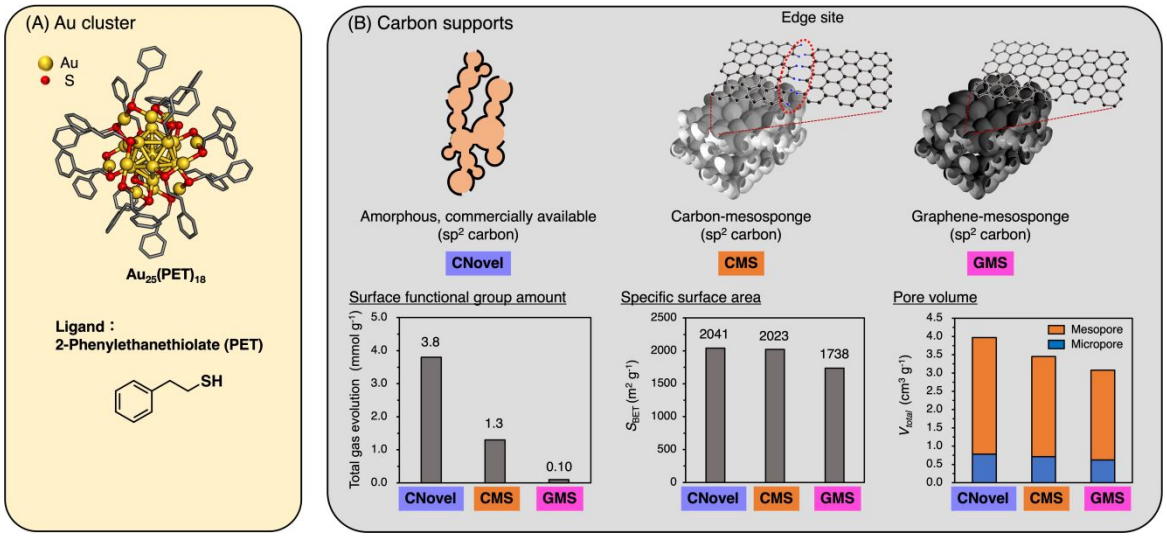

Fig 1. Precursors used in this study for the synthesis of heterogeneous Au cluster catalysts. (A) Single crystal structure of $[Au_{25}(PET)_{18}]^0$. (B) Schematic representations and properties of the carbon supports. Mesopore of CNovel is coloured in orange in the scheme.

$[Au_{25}(PET)_{18}]^0$ was successfully adsorbed onto the carbon support. Hereinafter, the composites thus obtained are referred to as $Au_{25}(PET)_{18}$/C, where C represents the carbon support (CNovel, CMS or GMS).

$Au_{25}(PET)_{18}$/C composites were calcined at the calcination temperature (T_{cal}) of 325, 350, 375, 400 and 425 ℃ for 12 h to create active sites by partial removal of the PET ligands. The resulting catalysts after calcination are referred to as $Au_{25}(PET)$/C. The extent of PET removal was monitored by the catalytic activity in the aerobic oxidation of 1-phenylethanol to acetophenone (Fig. S5).[34] While all the $Au_{25}(PET)_{18}$/C composites showed almost no activity due to the full ligation, the catalytic activity increased with T_{cal}. Interestingly, the threshold T_{cal} at which the activity appeared depended on the carbon support. Specifically, $Au_{25}(PET)$/CMS and $Au_{25}(PET)$/GMS started to show moderate reactivity at T_{cal} = 350 and 375 ℃, respectively, while $Au_{25}(PET)$/CNovel showed lower activity even at T_{cal} = 425 ℃. This result indicates that more heating is required to remove PET on CNovel.

Most of $Au_{25}(PET)$/C did not show the diffraction peak corresponding to metallic Au with face-centered cubic (fcc) structure in the powder X-ray diffraction (PXRD) patterns (Fig. S6), indicating that no drastic aggregation occurred during calcination. On the other hand, $Au_{25}(PET)$/CMS and $Au_{25}(PET)$/GMS prepared at T_{cal} = 425 ℃ showed a small hump at ~38° assigned to the diffraction of (111) planes of fcc Au, suggesting thermally induced aggregation of Au_{25}. In contrast, no such a hump was observed for $Au_{25}(PET)$/CNovel prepared at T_{cal} = 425 ℃. Based on these results, the T_{cal} was determined as the highest temperature at which $Au_{25}(PET)$/C exhibited catalytic activity without aggregation: 425, 375 and 400 ℃ for C = CNovel, CMS and GMS, respectively. These optimized calcination temperatures were significantly higher than the temperature at which the PET ligands were completely removed from $Au_{25}(PET)_{18}$ in the powder form (Fig. S1C). This result indicates that the PET ligands are difficult to desorb from $Au_{25}(PET)_{18}$ adsorbed on carbon supports due to non-covalent ligand-support interactions.[34]

Next, the calcination time (t_{cal}) was optimized at each optimized T_{cal} so that the AuNCs on the resulting $Au_{25}(PET)$/C have similar structures regardless of the carbon support. First, the structures of the AuNCs on $Au_{25}(PET)$/C were investigated in terms of the coordination numbers of Au–Au bonds (CN_{Au-Au}) and Au–S bonds (CN_{Au-S}) determined by the Au L_3-edge X-ray absorption fine structure (XAFS) analysis (Fig. S7). The X-ray near-edge structure (XANES) spectra of $Au_{25}(PET)_{18}$/C were mostly featureless before calcination, while the peaks corresponding to metallic Au developed for all $Au_{25}(PET)$/C with increasing t_{cal} (Fig. S7A). The extended XAFS

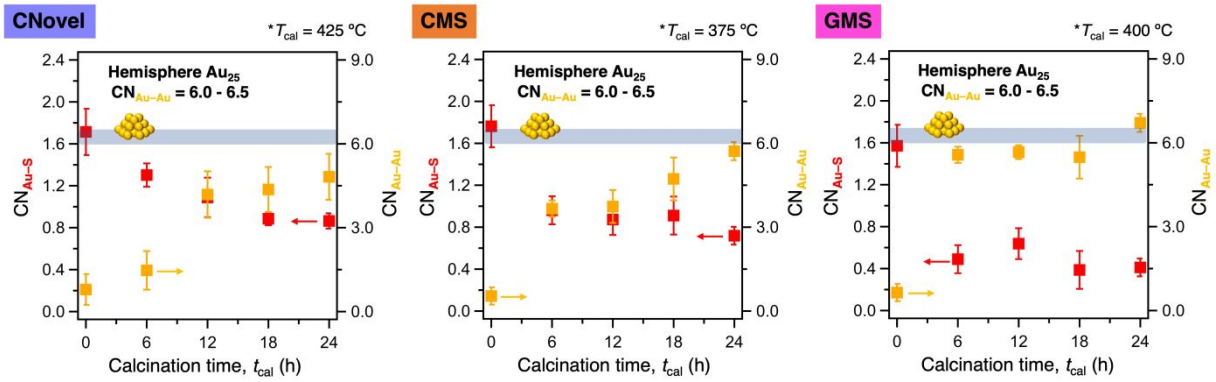

Fig. 2 The CN_{Au-S} (red) and CN_{Au-Au} (yellow) values of $Au_{25}(PET)_{18}$/C obtained after calcination for t_{cal} (h), estimated from curve-fitting analyses of Au L_3-edge EXAFS oscillations.

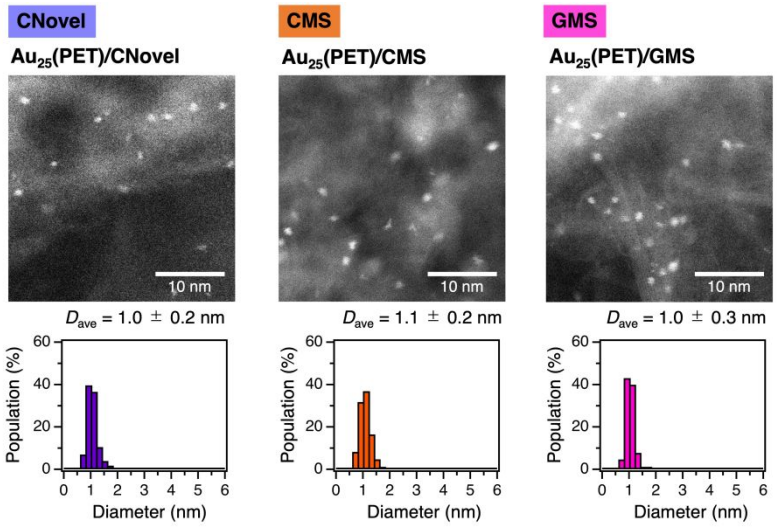

Fig. 3 Typical AC-HAADF-STEM images and size distributions of **$Au_{25}(PET)$/C** with C = CNovel, CMS, and GMS.

(EXAFS) oscillations and their Fourier transforms of Au_{25}(PET)/C are shown in Fig. S7B, C and D, respectively. The CN_{Au-Au} and CN_{Au-S} values (Table S2) are plotted as a function of t_{cal} in Fig. 2. The CN_{Au-S} values of $Au_{25}(PET)_{18}$/C were 1.6–1.8, independent of C, which are comparable to that estimated from the crystal structure of $Au_{25}(PET)_{18}$ (1.4).[66] In contrast, the CN_{Au-Au} values of $Au_{25}(PET)_{18}$/C were 0.5–0.8, significantly smaller than that estimated from the crystal structure (3.3). This underestimation was previously attributed to the thermal fluctuation of the Au_{13} core at room temperature.[66] At t_{cal} = 6 h, the CN_{Au-S} decreased while the CN_{Au-Au} increased, suggesting the gradual removal of PET ligands and growth of the Au cores independent of C. For C = CMS and GMS, the CN_{Au-S} and CN_{Au-Au} values remained almost constant during t_{cal} = 6–12 h, while the CN_{Au-Au} value increased due to aggregation by prolonged calcination. Nevertheless, the CN_{Au-Au} values were smaller or comparable to those theoretically calculated from the model structure of hemispherical Au_{25} in the fcc structure (6.0–6.5). Thus, the severe aggregation was unlikely to occur even at t_{cal} = 24 h. For C = CNovel, the gradual change of CN_{Au-S} and CN_{Au-Au} values continued until t_{cal} = 18 h and remained almost constant at t_{cal} > 18 h. Second, the structures of the Au NCs on Au_{25}(PET)/C were investigated in terms of the catalytic activity for 1-phenylethanol oxidation. As shown in Fig. S8, the activity was significantly enhanced at t_{cal} = 12 h for C = CNovel and at t_{cal} = 6 h for C = CMS and GMS. Based on the above two results, Au_{25}(PET)/C suitable for the study of carbon effects on catalysis were prepared at (T_{cal}, t_{cal}) = (425 ℃, 18 h), (375 ℃, 12 h) and (400 ℃, 12 h) for C = CNovel, CMS and GMS, respectively. As summarized in Table S3, the structural parameters of Au NCs on Au_{25}(PET)/C prepared under the above calcination conditions are comparable. In the following, the Au_{25}(PET)/C obtained under the optimized conditions are shown in bold: **Au_{25}(PET)/CNovel**, **Au_{25}(PET)/CMS** and **Au_{25}(PET)/GMS** were prepared under the calcination conditions of (T_{cal}, t_{cal}) = (425 ℃, 18 h), (375 ℃, 12 h) and (400 ℃, 12 h), respectively.

The size of AuNCs on **Au_{25}(PET)/C** was further characterized by aberration-corrected high-angle annular dark-field scanning transmission electron microscopy (AC-HAADF-STEM). Typical images and size distributions of AuNCs for each **Au_{25}(PET)/C** are shown in Fig. 3. The average particle sizes of **Au_{25}(PET)/C** were similar regardless of C: 1.0 ± 0.2, 1.1 ± 0.2 and 1.0 ± 0.3 nm for C = CNovel, CMS and GMS, respectively. These sizes retained the original sizes of $Au_{25}(PET)_{18}$/C (1.0 ± 0.2 nm, Fig. S9) prepared by the adsorption of $Au_{25}(PET)_{18}$ on the carbon supports in the intact form.[47] Based on the obtained results of the catalytic activity, PXRD, XAFS and AC-HAADF-STEM, we concluded that the partially thiolated, atomically precise Au_{25} NCs with similar structure are formed on **Au_{25}(PET)/C** on each carbon support.

Aqueous-phase ester synthesis

The catalytic performance of **Au_{25}(PET)/C** in water was investigated in the aerobic oxidation of $PhCH_2OH$ (**1**, Fig. 4 and Table S4) as a model reaction. The products obtained were the target compound ($PhCO_2CH_2Ph$; **2**) and benzaldehyde (PhCHO; **3**) and benzoic acid (PhCOOH; **4**) as by-products. The time course of the conversion of **1** and the yields of products **2–4** are plotted in Fig. 4 and are summarized in Table S4. When **Au_{25}(PET)/CNovel** and **Au_{25}(PET)/CMS** were used, **4** was the main product throughout the reaction and the maximum yield of **2** was only 28 ± 1% and 26 ± 1%, respectively. In contrast, **Au_{25}(PET)/GMS** gave a higher yield of **2** than **4** at the initial stage (0–40 min) and took the maximum yield of 39 ± 1% at 60 min. Although the yield of **2** decreased slightly as the reaction time was prolonged, the maximum yield was higher than those obtained for **Au_{25}(PET)/CNovel** and **Au_{25}(PET)/CMS**. These results illustrate that the property of the carbon support determines the selectivity of esters in alcohol oxidation in water since the active Au NCs on each carbon support have similar structures. To highlight the importance of the carbon support for ester formation, the activity and selectivity in the oxidation of **1** by **Au_{25}(PET)/GMS** were compared with partially-thiolated Au_{25} NCs on hydrotalcite (Au_{25}(*p*MBA)/Mg_3Al; *p*MBA = *p*-mercaptobenzoic acid)[54] and ligand-free Au_{25} NCs on double metal hydroxide composed of Co and Ce (Au_{25}/Co_3Ce).[67] As shown in Fig. S10, the yields of **2** by Au_{25}(*p*MBA)/Mg_3Al and Au_{25}/Co_3Ce were negligibly small in contrast to **Au_{25}(PET)/GMS**. Although the activity of Au_{25}/Co_3Ce was much

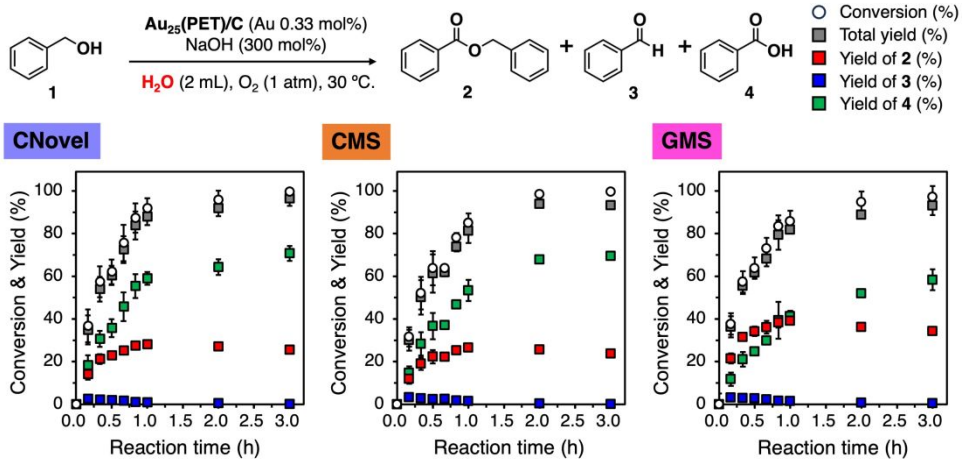

Fig. 4 Catalytic activity and selectivity of **Au_{25}(PET)/C** for the oxidation of benzyl alcohol (**1**) in H_2O. Reaction conditions: **1** (Au 0.33 mol%), **Au_{25}(PET)/C** (5.0 mg), NaOH (300 mol%), H_2O (2 mL), O_2 (1 atm, balloon), 30 ℃. The error bar on each data point corresponds to the standard deviations of the results obtained from three independent measurements.

higher than the others, the selectivity to **2** was negligibly small throughout the time course of the reaction, as reported previously.[67]

The highest selectivity to **2** by **Au_{25}(PET)/GMS** is due to the specific nature of GMS, as the Au_{25} active sites on it were common to those on other **Au_{25}(PET)/C** (Table S3). Mechanistic studies were performed to elucidate the origin of the higher selectivity to **2** by **Au_{25}(PET)/GMS** than **Au_{25}(PET)/CMS** or **Au_{25}(PET)/CNovel**. First, we considered the possibility that the hydrolysis of product **2** to **4** is most retarded on GMS.[34,40,54,67] To test this hypothesis, the conversion in the hydrolysis of **2** in basic water in the presence or absence of **Au_{25}(PET)/C** was compared. As shown in Fig. S11 and Table S5, all **Au_{25}(PET)/C** suppressed the hydrolysis of **2**, probably due to the adsorption on the carbon surface. However, the support-dependent suppression of the hydrolysis of **2** does not explain the highest yield of **2** by **Au_{25}(PET)/GMS**, since the activity was in the order of CMS > GMS > CNovel, suggesting that **Au_{25}(PET)/CNovel** suppressed the ester hydrolysis the most. We, then, considered two scenarios for the efficient formation of **2** on GMS: (i) promotion of the formation of **2** by nucleophilic attack of $\mathbf{1}^-$ to PhCHO (**3**) ($\mathbf{1}^-$ + **3** → **2** + H_2O); (ii) suppression of the competing process of formation of the unwanted **4** by nucleophilic attack of OH^- to **3** (OH^- + **3** → **4** + H_2O). To gain insight into which process is important, the adsorption of

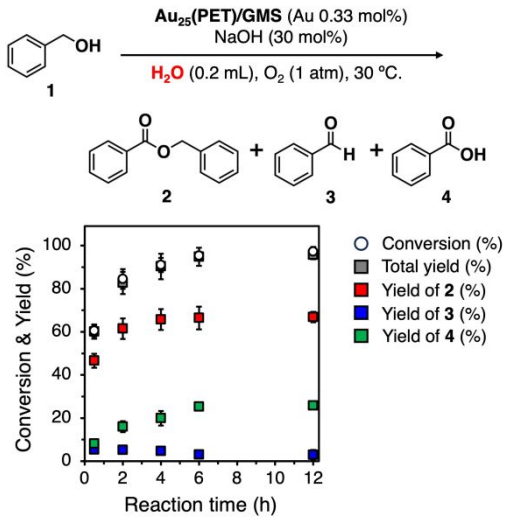

Fig. 5 Time course of the catalytic activity and selectivity of the oxidation of **1** by **Au_{25}(PET)/GMS** in basic water under the following optimized conditions: **1** (Au 0.33 mol%), **Au_{25}(PET)/GMS** (5.0 mg), NaOH (30 mol%), H_2O (0.2 mL), O_2 (1 atm, balloon), 30 °C. The error bar on each data point correspond to the standard deviations of the results obtained from three independent measurements.

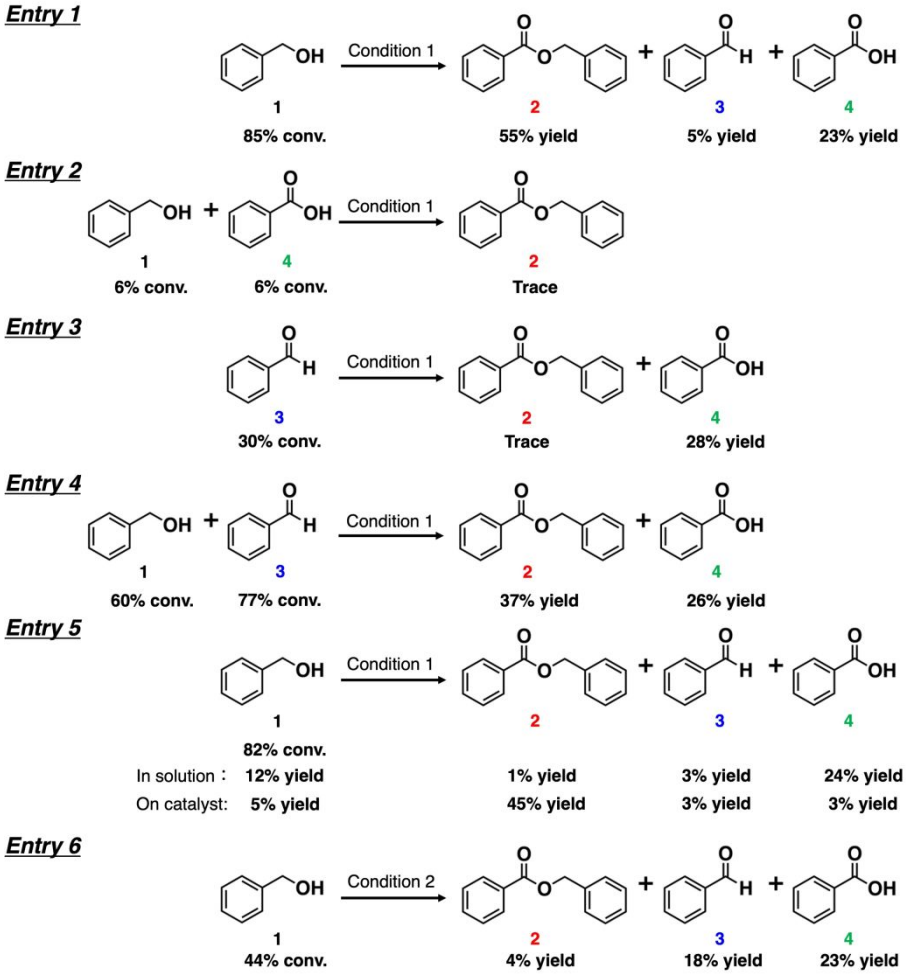

Scheme 2 Possible formation processes of **2** from **1** catalysed by **Au_{25}(PET)/GMS**. Condition 1: Substrate (**1** for Au 0.33 mol% or **1** and **3**/**4** for Au 0.66 mol% each), **Au_{25}(PET)/GMS** (5.0 mg), NaOH (30 mol%), H_2O (2 mL), O_2 (1 atm, balloon), 30 °C, 12 h. Condition 2: MeCN (1.8 mL) and H_2O (0.2 mL) instead of H_2O (2 mL).

deprotonated $PhCH_2OH$ ($PhCH_2O^-$; $\mathbf{1}^-$) and products **2–4** on the three carbons was compared in basic water (Fig. S12 and Table S6). Based on the adsorption property of **3**, scenario (i) was effective in the order of CMS > GMS > CNovel, as hydrophilic OH^- in the solution is prevented from accessing the hydrophobic carbon surface. Since **3** in the solution is likely to be attacked by hydrophilic OH^- from the solution, scenario (ii) is also effective in the order of CMS > GMS > CNovel. Finally, the hydrophobicity of CNovel, CMS and GMS supports was compared by measuring their water-vapour adsorption isotherms (Fig. S13A). Since the adsorption of clustered water molecules starts at a relative pressure (P/P_0) > 0.7, the adsorption isotherm was compared at P/P_0 < 0.6 (Fig. S13B).[58,68] The amount of adsorbed water was in the order of CNovel > CMS > GMS, which is parallel to the order of the amount of functional groups (Fig. 1). This result indicates that **2** and **3** adsorbed on the most hydrophobic GMS are most efficiently protected from hydrolysis and nucleophilic attack by OH^- for the formation of unwanted **4**. Therefore, the highest yield of **2** by **Au_{25}(PET)/GMS** can be explained by considering the contribution of all the factors discussed above. In conclusion, the GMS support promotes the ester formation ($\mathbf{1}^-$ + **3** → **2** + H_2O) and suppresses the formation of unwanted **4** (OH^- + **3** → **4** + H_2O) due to the moderate adsorption ability of **3** on the GMS surface, as well as the suppression of hydrolysis of the formed ester in basic water than other carbon supports due to higher hydrophobicity.

The yield of **2** in water by **Au_{25}(PET)/GMS** was attempted to be maximized by optimizing the reaction conditions, such as the amounts of NaOH and H_2O and the loading amount of AuNCs. First, the yield of **2** increased by reducing the amount of NaOH from 500 to 30% although the reaction rate decreased (Fig. S13A). The yield of **2** after 12 h increased from 42 to 55% when the amount of NaOH was reduced from 75 to 30 mol% (Fig. S13B), while it decreased to 39% when the amount of NaOH was further reduced to 10 mol%. The retardation of the reaction at small amounts of NaOH is due to the consumption of NaOH to neutralize by-product **4**. Second, when the amount of H_2O was reduced from 2 mL to 0.2 mL at 30 mol% NaOH, the yield of **2** increased from 55 to 67% after 12 h (Fig. S14). Third, the loading of the Au_{25} NCs was changed from 1 wt%. After adsorbing 0.2 or 2 wt% of $[Au_{25}(PET)_{18}]^0$ on GMS (Fig. S15), they were calcined under the optimized conditions (T_{cal}, t_{cal}) = (400 °C, 12 h) used for 1 wt% catalyst. The Au_{25} NCs underwent aggregation at 2 wt% loading, based on the results that the CN_{Au-Au} value (7.4 ± 0.6) became larger than the theoretical value for a hemispherical Au_{25} in fcc structure (6.0–6.5) (Fig. S16 and Table S7) and that a small hump was observed in PXRD (Fig. S17). The average size of AuNCs estimated by AC-HAADF-STEM measurement (Fig. S19) was 1.4 ± 0.4 nm, which is also larger than that of the pristine $Au_{25}(PET)_{18}$ (1.0 ± 0.2 nm, Fig. S9), supporting the aggregation to some extent. Reducing the loading to 0.2 wt% resulted in a significant decrease in the yield of **2**, while increasing the loading to 2 wt% maintained the yield of **2** at 66% (Fig. S18). By using the above optimized conditions, we achieved a high selectivity towards ester formation under aqueous conditions, as summarized in Fig. 5 and Table S8. The catalysts could be recycled while maintaining the highest selectivity to **2**, although the activity gradually decreased upon the recycling (Fig. S21). The AC-HAADF-STEM measurement of **Au_{25}(PET)/GMS** after six cycles showed that the average diameter of AuNCs slightly increased from 1.0 ± 0.3 nm to 1.3 ± 0.4 nm (Fig. S22). This growth of AuNCs would not be a major cause of deactivation since we have reported that the Au_{144}/C with an average diameter of 1.6 nm showed higher activity than the Au_{25}/C with an average diameter of 1.0 nm.[40] A more plausible cause is the contamination from the acetone used as a solvent to extract the product. This speculation is supported by the gradual increase in the yield of **3** (Fig. S21): the use of MeCN as a solvent instead of water significantly decreased the activity and the yield of **2**, while increasing the yield of **3** (Entry 6 of Scheme 2).

The main route of formation of **2** by oxidation of **1** under the optimized aqueous conditions was attempted to be identified by the mechanistic studies. Here, the volume of H_2O was increased from 0.2 mL (Fig. 5 and Table S8) to 2 mL to completely dissolve the reactants except for **2**, although the yield of **2** was slightly reduced from 64 to 55 % (Entry 1 in Scheme 2 and Fig. S14). The other conditions were the same as those optimized in Fig. 5. Considering the basic condition, the formation of **2** via Fisher esterification (dehydrative coupling between **1** and **4**)[7] is unlikely. In fact, only a trace amount of **2** was obtained when **1** and **4** were used as reactants (Entry 2). On the other hand, **2** was not formed by the homocoupling of the aldehydes **3**:[69,70]

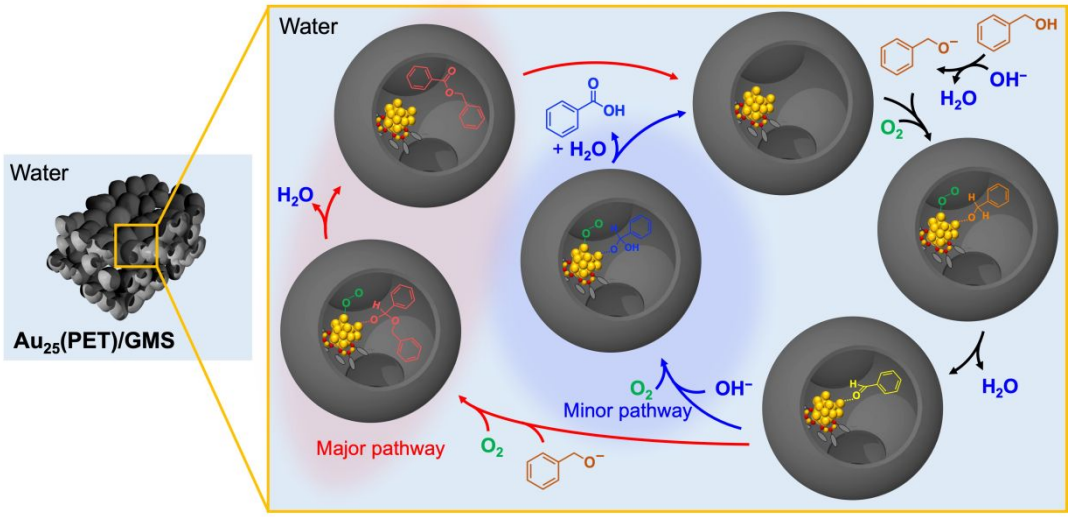

Scheme 3. Proposed mechanism for benzyl benzoate synthesis from benzyl alcohol catalysed by **Au_{25}(PET)/GMS** in aqueous phase.

only **4** was formed with 28% yield from **3** as the reactant (Entry 3). The addition of **1** to Entry 3 increased the yield of **2** to 37% (Entry 4). Thus, the coupling between **1** and **3** is the main pathway for the formation of **2**. The formed **2** was mainly adsorbed on the catalyst (Entry 5), which is consistent with the adsorption property observed using the pristine support (Fig. S12) and suggests the suppression of hydrolysis of **2** during the reaction. Finally, the solvent was changed from 2 mL H_2O to 1.8 mL MeCN and 0.2 mL H_2O to evaluate the importance of water. The yield of **2** was significantly reduced to 4% and **3** and **4** were formed as the main products (Entry 6). This result also supports that adsorption properties in the aqueous phase play a key role in the selective synthesis of **2**, as all substrates are likely to be unadsorbed on the GMS support under the present conditions due to the higher solubility of **1**-**4** in organic solvent.

Based on these mechanistic studies, we propose a plausible reaction mechanism in Scheme 3. The reactant $PhCH_2O^-$ (**1^-**), formed by deprotonation of **1** by the base, is first coordinated to the Au_{25} NC, followed by the oxidation to **3** on the Au_{25} NC surface. Although the formed **3** can react with either **1^-** or OH^-, the hydrophobic nature of the carbon pores promotes the reaction of **1^-** while suppressing the approach of OH^-. This selectivity results in the formation of **2** as the main pathway. In addition, the formed **2** is stabilized on the carbon against hydrolysis in the aqueous phase due to its higher affinity to the carbon and low solubility in H_2O. The GMS support provides the reaction environment for efficient ester formation (**1^-** + **3** → **2** + H_2O) in water and suppresses the hydrolysis of **2** (**2** + H_2O → **1^-** + **3**). These unique properties of GMS arise from the moderate adsorption properties of each substrate and product and due to the very low amount of the surface functional groups (Fig. 1B) and limited water adsorption due to high hydrophobicity (Fig. S13).

Conclusions

In conclusion, we synthesized identical partially thiolated Au_{25} nanocluster catalysts on three types of carbon supports, GMS, CMS, and CNovel. The GMS-supported Au_{25} nanocluster exhibited the highest yield of benzyl benzoate in the aqueous phase alcohol oxidation than the CMS or CNovel-supported catalyst. The density of the Au nanocluster, the amount of NaOH added, and the water-to-catalyst ratio play important roles in the benzyl benzoate selectivity. The yield was up to 67% under the optimized conditions. Mechanistic studies suggested that the adsorption of benzyl alkoxide and benzaldehyde, while suppressing the approach of hydroxide ions, improved the selectivity by avoiding the unfavorable benzoic acid formation and hydrolysis of the as-formed benzyl benzoate. This work proposes an environmentally friendly approach for ester synthesis in the aqueous phase by utilizing the synergistic effect of Au nanocluster and carbon support.

Experimental

All methods are summarized in the ESI file.

Author contributions

K. S. conducted most of the experiments and analyses. K. C. synthesized CMS and GMS carbon supports, conducted N_2 adsorption/desorption and TPD-MS measurements and analysed the data. S. M. performed AC-HAADF-STEM measurements and advised in some experiments. S. M., T. Y., H. N. and T. T. supervised the project. The manuscript was first written by K. S. through discussions among all the authors, and all approved the final version.

Conflicts of interest

There are no conflicts to declare.

Data availability

The data supporting this article have been included as part of the ESI. Additional data that support the findings of this study are available from the corresponding authors upon reasonable request.

Acknowledgements

This research was financially supported by JST, CREST (grant no. JPMJCR20B2), “Advanced Research Infrastructure for Materials and Nanotechnology in Japan (ARIM)” of the Ministry of Education, Culture, Sports, Science and Technology (MEXT) (Grant Number JPMXP1224UT0045), a Grant-in-Aid for Scientific Research (A) (Grant No. JP23H00284), for Early-Career Scientists (Grant No. JP21K14476 and JP23K13617) and for JSPS Fellows (Grant No. JP24KJ0676) from the Japan Society for the Promotion of Science (JSPS) and the World-leading Innovative Graduate Study Program for Materials Research, Information, and Technology (MERIT-WINGS) from the University of Tokyo. The synchrotron radiation experiments were performed under the approval of Japan Synchrotron Radiation Research Institute (JASRI) (proposal no. 2023A1635 and 2024A1734). This work was performed under the Cooperative Research Program of “Network Joint Research Center for Materials and Devices (MEXT)”.

References

1 J. Otera, *Chem. Rev.*, 1993, **93**, 1449–1470.
2 S. G. Ouellet, A. M. Walji and D. W. C. Macmillan, *Acc. Chem. Res.*, 2007, **40**, 1327–1339.
3 C. M. Thomas, *Chem. Soc. Rev.*, 2009, **39**, 165–173.
4 C. Zheng and S.-L. You, *Chem. Soc. Rev.*, 2012, **41**, 2498–2518.
5 R. Takise, K. Muto and J. Yamaguchi, *Chem. Soc. Rev.*, 2017, **46**, 5864–5888.
6 G. S. Yedase, S. Venugopal, A. P. and V. R. Yatham, *Asian J. Org. Chem.*, 2022, **11**, e202200478.
7 Z. Khan, F. Javed, Z. Shamair, A. Hafeez, T. Fazal, A. Aslam, W. B. Zimmerman and F. Rehman, *J. Ind. Eng. Chem.*, 2021, **103**, 80–101.
8 R. L. Oliveira, P. K. Kiyohara and L. M. Rossi, *Green Chem.*, 2009, **11**, 1366–1370.
9 K. Suzuki, T. Yamaguchi, K. Matsushita, C. Iitsuka, J. Miura, T. Akaogi and H. Ishida, *ACS Catal.*, 2013, **3**, 1845–1849.
10 A. Abad, A. Corma and H. García, *Chem. Eur. J.*, 2007, **14**, 212–222.
11 P. Fristrup, L. B. Johansen and C. H. Christensen, *Catal. Lett.*, 2008, **120**, 184–190.

12 T. Mitsudome, A. Noujima, T. Mizugaki, K. Jitsukawa and K. Kaneda, *Adv. Synth. Catal.*, 2009, **351**, 1890–1896.
13 M. Conte, H. Miyamura, S. Kobayashi and V. Chechik, *J. Am. Chem. Soc.*, 2009, **131**, 7189–7196.
14 B. Donoeva, N. Masoud and P. E. de Jongh, *ACS Catal.*, 2017, **7**, 4581–4591.
15 D. Muñoz‐Santiburcio, M. F. Camellone and D. Marx, *Angew. Chem., Int. Ed.*, 2018, **57**, 3327–3331.
16 A. Mahdavi-Shakib, J. Sempel, L. Babb, A. Oza, M. Hoffman, T. N. Whittaker, B. D. Chandler and R. N. Austin, *ACS Catal.*, 2020, **10**, 10207–10215.
17 S. Hasegawa, S. Takano, K. Harano and T. Tsukuda, *JACS Au*, 2021, **1**, 660–668.
18 T. Mitsudome, A. Noujima, T. Mizugaki, K. Jitsukawa and K. Kaneda, *Green Chem.*, 2009, **11**, 793–797.
19 B. N. Zope, D. D. Hibbitts, M. Neurock and R. J. Davis, *Science*, 2010, **330**, 74–78.
20 C. D. Pina, E. Falletta and M. Rossi, *Chem. Soc. Rev.*, 2011, **41**, 350–369.
21 J. C. F. Rodríguez-Reyes, C. M. Friend and R. J. Madix, *Surf. Sci.*, 2012, **606**, 1129–1134.
22 S. E. Davis, M. S. Ide and R. J. Davis, *Green Chem.*, 2012, **15**, 17–45.
23 S. Rautiainen, O. Simakova, H. Guo, A.-R. Leino, K. Kordás, D. Murzin, M. Leskelä and T. Repo, *Appl. Catal. A: Gen.*, 2014, **485**, 202–206.
24 H. Weerathunga, S. Sarina, H.-Y. Zhu and E. R. Waclawik, *ACS Omega*, 2021, **6**, 4740–4748.
25 A. Taketoshi, Y. Gangarajula, R. Sodenaga, A. Nakayama, M. Okumura, N. Sakaguchi, T. Murayama, T. Shimada, S. Takagi, M. Haruta, B. Qiao, J. Wang and T. Ishida, *ACS Appl. Mater. Interfaces*, 2023, **15**, 34290–34302.
26 R. H. Valivety, G. A. Johnston, C. J. Suckling and P. J. Halling, *Biotechnol. Bioeng.*, 1991, **38**, 1137–1143.
27 Y.-Y. Linko, M. Lämsä, A. Huhtala and O. Rantanen, *J. Am. Oil Chem.' Soc.*, 1995, **72**, 1293–1299.
28 K. Manabe, S. Iimura, X.-M. Sun and S. Kobayashi, *J. Am. Chem. Soc.*, 2002, **124**, 11971–11978.
29 Z. Guo and Y. Sun, *Biotechnol. Prog.*, 2004, **20**, 500–506.
30 P.-Y. Stergiou, A. Foukis, M. Filippou, M. Koukouritaki, M. Parapouli, L. G. Theodorou, E. Hatziloukas, A. Afendra, A. Pandey and E. M. Papamichael, *Biotechnol. Adv.*, 2013, **31**, 1846–1859.
31 V. Singhania, M. Cortes-Clerget, J. Dussart-Gautheret, B. Akkachairin, J. Yu, N. Akporji, F. Gallou and B. H. Lipshutz, *Chem. Sci.*, 2021, **13**, 1440–1445.
32 Y. Zheng, C. Huang, Y. Li, Y. Yang and R. Xu, *ChemCatChem*, 2024, **16**, e202300976.
33 T. Yoskamtorn, S. Yamazoe, R. Takahata, J. Nishigaki, A. Thivasasith, J. Limtrakul and T. Tsukuda, *ACS Catal.*, 2014, **4**, 3696–3700.
34 K. Sakamoto, S. Masuda, S. Takano and T. Tsukuda, *ACS Catal.*, 2023, **13**, 3263–3271.
35 Z. Dou, Z. Xu, T. Zhang, S. Li, C. Xu, T. Fan and H. Guo, *Resour. Chem. Mater.*, 2023, **2**, 117–127.
36 M. Turner, V. B. Golovko, O. P. H. Vaughan, P. Abdulkin, A. Berenguer-Murcia, M. S. Tikhov, B. F. G. Johnson and R. M. Lambert, *Nature*, 2008, **454**, 981–983.
37 D. P. Anderson, J. F. Alvino, A. Gentleman, H. A. Qahtani, L. Thomsen, M. I. J. Polson, G. F. Metha, V. B. Golovko and G. G. Andersson, *Phys. Chem. Chem. Phys.*, 2013, **15**, 3917–3929.
38 R. Jin, C. Zeng, M. Zhou and Y. Chen, *Chem. Rev.*, 2016, **116**, 10346–10413.
39 B. Zhang, J. Fang, J. Li, J. J. Lau, D. Mattia, Z. Zhong, J. Xie and N. Yan, *Chem. Asian J.*, 2016, **11**, 532–539.
40 S. Yamazoe, T. Yoskamtorn, S. Takano, S. Yadnum, J. Limtrakul and T. Tsukuda, *Chem. Rec.*, 2016, **16**, 2338–2348.
41 I. Chakraborty and T. Pradeep, *Chem. Rev.*, 2017, **117**, 8208–8271.
42 R. R. Nasaruddin, T. Chen, N. Yan and J. Xie, *Coord. Chem. Rev*, 2018, **368**, 60–79.
43 R. R. Nasaruddin, Q. Yao, T. Chen, M. J. Hülsey, N. Yan and J. Xie, *Nanoscale*, 2018, **10**, 23113–23121.
44 J. Yan, B. K. Teo and N. Zheng, *Acc. Chem. Res.*, 2018, **51**, 3084–3093.
45 S. Tian, Y. Cao, T. Chen, S. Zang and J. Xie, *Chem. Commun.*, 2019, **56**, 1163–1174.
46 V. Sudheeshkumar, K. O. Sulaiman and R. W. J. Scott, *Nanoscale Adv*, 2020, **2**, 55–69.
47 T. Kawawaki, Y. Kataoka, M. Hirata, Y. Iwamatsu, S. Hossain and Y. Negishi, *Nanoscale Horiz.*, 2021, **6**, 409–448.
48 M. H. Naveen, R. Khan and J. H. Bang, *Chem. Mater.*, 2021, **33**, 7595–7612.
49 R. H. Adnan, J. M. L. Madridejos, A. S. Alotabi, G. F. Metha and G. G. Andersson, *Adv. Sci.*, 2022, **9**, 2105692.
50 S. Li, X. Du, Z. Liu, Y. Li, Y. Shao and R. Jin, *Precis. Chem.*, 2023, **1**, 14–28.
51 W. Jing, H. Shen, R. Qin, Q. Wu, K. Liu and N. Zheng, *Chem. Rev.*, 2023, **123**, 5948–6002.
52 B. Zhang, C. Xia, J. Hu, H. Sheng and M. Zhu, *Nanoscale*, 2023, **16**, 1526–1538.
53 Z. Liu, X.-M. Yang, Y. Wang and S. Wang, *Nano Res.*, 2025, **18**, 94907141.
54 S. Masuda and T. Tsukuda, *ACS Catal.*, 2023, 16179–16187.
55 K. Sakamoto, S. Masuda, S. Takano and T. Tsukuda, *Nanoscale*, 2024, **16**, 20608–20616.
56 J.-H. Zhou, Z.-J. Sui, J. Zhu, P. Li, D. Chen, Y.-C. Dai and W.-K. Yuan, *Carbon*, 2007, **45**, 785–796.
57 H. Nishihara, T. Simura, S. Kobayashi, K. Nomura, R. Berenguer, M. Ito, M. Uchimura, H. Iden, K. Arihara, A. Ohma, Y. Hayasaka and T. Kyotani, *Adv. Funct. Mater.*, 2016, **26**, 6418–6427.
58 H. Nishihara, H.-W. Zhao, K. Kanamaru, K. Nomura, M. Ohwada, M. Ito, L.-X. Li, B.-G. An, T. Horikawa and T. Kyotani, *Carbon Reports*, 2022, **1**, 123–135.
59 W. Yu, T. Yoshii, A. Aziz, R. Tang, Z. Pan, K. Inoue, M. Kotani, H. Tanaka, E. Scholtzová, D. Tunega, Y. Nishina, K. Nishioka, S. Nakanishi, Y. Zhou, O. Terasaki and H. Nishihara, *Adv. Sci.*, 2023, **10**, 2300268.
60 M. A. Tofanelli, K. Salorinne, T. W. Ni, S. Malola, B. Newell, B. Phillips, H. Häkkinen and C. J. Ackerson, *Chem. Sci.*, 2016, **7**, 1882–1890.
61 M. Zhu, W. T. Eckenhoff, T. Pintauer and R. Jin, *J. Phys. Chem. C*, 2008, **112**, 14221–14224.
62 T. Ishii, S. Kashihara, Y. Hoshikawa, J. Ozaki, N. Kannari, K. Takai, T. Enoki and T. Kyotani, *Carbon*, 2014, **80**, 135–145.
63 K. Wakabayashi, T. Yoshii and H. Nishihara, *Carbon*, 2023, **210**, 118069.
64 T. Xia, T. Yoshii, K. Nomura, K. Wakabayashi, Z.-Z. Pan, T. Ishii, H. Tanaka, T. Mashio, J. Miyawaki, T. Otomo, K. Ikeda, Y. Sato, M. Terauchi, T. Kyotani and H. Nishihara, *Chem. Sci.*, 2023, **14**, 8448–8457.
65 K. Kaneko and C. Ishii, *Colloids Surf.*, 1992, **67**, 203–212.
66 S. Yamazoe, S. Takano, W. Kurashige, T. Yokoyama, K. Nitta, Y. Negishi and T. Tsukuda, *Nat. Commun.*, 2016, **7**, 10414.
67 S. Masuda, S. Takano, S. Yamazoe and T. Tsukuda, *Nanoscale*, 2022, **14**, 3031–3039.
68 A. Yoshida, K. Pirabul, S. Fujii, Z.-Z. Pan, T. Yoshii, M. Ito, K. Izawa, Y. Minegishi, Y. Noguchi, N. Hiyoshi, K. Takeda, Y. Hasegawa, T. Itoh and H. Nishihara, *ACS Appl. Mater. Interfaces*, 2024, **16**, 50115–50124.
69 T. Seki, T. Nakajo and M. Onaka, *Chem. Lett.*, 2006, **35**, 824–829.
70 R. Dhanya, T. Shilpa, S. Saranya and G. Anilkumar, *ChemistrySelect*, 2020, **5**, 754–763.

Data availability statement

The data supporting this article have been included as part of the ESI. Additional data that support the findings of this study are available from the corresponding authors upon reasonable request.